Available online at www.sciencedirect.com
ScienceDirect
Scripta Materialia 55 (2006) 1083–1086
Scripta MATERIALIA
www.actamat-journals.com

Composites by aluminum infiltration of porous silicon carbide derived from wood precursors

T.E. Wilkes,[a] M.L. Young,[a] R.E. Sepulveda,[b] D.C. Dunand[a] and K.T. Faber[a,*]

[a] *Department of Materials Science and Engineering, Robert R. McCormick School of Engineering and Applied Science, Northwestern University, 2220 Campus Drive, Evanston, IL 60208-3108, United States*
[b] *Departamento de Física de la Materia Condensada, Universidad de Sevilla, CP 41012, Seville, Spain*

Received 19 May 2006; revised 17 August 2006; accepted 21 August 2006
Available online 22 September 2006

Composites were fabricated by infiltration of molten Al–13Si–9Mg into porous SiC derived from wood. The composite microstructure retains the heterogeneous orthorhombic symmetry of the initial wood material. As compared to the uninfiltrated SiC preform, the composite shows much improved transverse compressive strength and stiffness, resulting in reduced anisotropy.

Keywords: Silicon carbide; Elastic behavior; Aluminum alloys; Composites; Porous materials

Research into wood-derived ceramics has expanded from the first studies of pyrolyzed carbon templates and their reaction with silicon to form silicon carbide (SiC) [1]. Different precursors, including assorted tree species and fiberboard products, have been used to demonstrate the microstructural versatility of the resulting porous ceramics [2,3]. In addition to SiC, the investigation of various processing routes has led to TiC, ZrC, Al_2O_3, ZrO_2 and TiO_2 porous ceramics, all of whose microstructures are directly related to that of the original wood material [4–7].

The microstructure of wood is composed of various channel types, running in the axial and radial directions (Fig. 1), that provide pathways for the distribution of water and other nutrients [8]. In all woods, a majority of the channels are parallel to the axial direction, but the size and distribution of channels vary between species. In the axial direction, hardwoods contain a bimodal distribution of large diameter vessel channels and smaller diameter fiber channels [9]. Hardwoods also contain radially oriented channels (i.e., rays) that are approximately the same size as the fiber channels. Natural optimization has led to this complex, yet mechanically effective structure that presents an inexpensive and easily machined renewable resource. The wide array of wood species can be used to create ceramic materials with unique anisotropic pore structures suitable for a wide range of applications.

Wood-derived SiC (biomorphic SiC or bioSiC), the material used in the present research, is applicable as a light-weight structural material, catalyst support, heat exchanger, high-temperature molten metal filter and composite reinforcement [10]. Currently, research concerning composites based on bioSiC has focused on Si–SiC ceramic matrix composites (CMC) [11]. In the process of forming the bioSiC, the wood preform is pyrolyzed at 1000 °C in argon for 1 h. The resulting porous carbon is melt infiltrated with an excess of molten silicon at 1550 °C in vacuum. As the metal is wicked into the porous carbon, it reacts to form β-silicon carbide:

$$C + Si \rightarrow \beta\text{-SiC} \quad (1)$$

Upon cooling, excess Si remains in the smaller diameter channels of the SiC, forming a Si–SiC CMC with residual porosity corresponding to the large diameter channels [11]. While extensive research has been carried out on these Si–SiC composites [11], studies involving metallic matrices are limited to squeeze casting an aluminum–silicon alloy into the residual porosity of the Si–SiC CMC [12]. Correspondingly, there is a lack of research involving the fabrication of bioSiC-reinforced metal matrix composites (MMCs). Conversion of the Si–SiC CMC to porous bioSiC is accomplished by using acid to etch the excess Si out of the bioSiC channels. The remaining porous SiC structure has varying amounts

* Corresponding author. E-mail: k-faber@northwestern.edu

1359-6462/$ - see front matter
doi:10.1016/j.scriptamat.2006.08.040

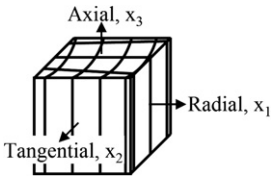

Figure 1. Schematic diagram of wood showing the three principle axes.

of unreacted carbon based on wood precursor microstructure [3] and infiltration time. By using the porous bioSiC as a preform, composites with metal matrices, such as aluminum, can be created by melt infiltration.

Both Al–SiC composites and melt infiltration, the material and process used in this study, have been extensively covered in literature [13]. In the present study, pressureless and pressurized melt infiltration are used to infiltrate porous bioSiC preforms with an aluminum–silicon–magnesium alloy. The microstructure and mechanical properties of the resulting composites are reported.

Beech wood (*Fagus sylvatica*), a hardwood, was pyrolyzed for 1 h in argon, resulting in porous carbon with the microstructure shown in Figure 2(a). After pyrolysis, the carbon was reacted with molten high-purity silicon (99.6 wt.% Si) at 1550 °C in vacuum for 1 h. After solidification of the resulting Si–SiC CMC, excess silicon was etched out of the channels with a 50/50 vol.% mixture of concentrated nitric and hydrofluoric acids.

Two bioSiC specimen sizes were used: $10 \times 10 \times 3$ mm^3 for pressureless infiltration and $25 \times 25 \times 10$ mm^3 for pressurized infiltration. The $10 \times 10 \times 3$ mm^3 specimens were used to test the viability of using the Lanxide PRIMEX™ pressureless metal infiltration method [14] to fabricate bioSiC-reinforced Al MMCs. The $25 \times 25 \times 10$ mm^3 samples were the largest possible pieces the infiltration apparatus, which is described below, could accommodate, and they were big enough to yield a sufficient number of $4 \times 4 \times 8$ mm^3 samples for mechanical testing.

Pressureless infiltration experiments followed procedures similar to the Lanxide PRIMEX™ pressureless metal infiltration method. A billet of Al–13Si–9Mg was placed on top of the specimens inside an alumina crucible that was heated in a tube furnace to 900 °C for 1 h. While 900 °C is well above the melting point of aluminum, it falls within the range (800–1200 °C) used in Lanxide experiments [15]. It has been shown that relatively high-temperatures were required to achieve adequate infiltration distances when using the PRIMEX™ process [16]. Experiments with two atmospheres were conducted: in vacuum and with ~0.1 MPa ultrahigh-purity nitrogen. The specific alloy used here has been shown to optimize wetting with SiC [17]. The Mg and Si additions improve the wetting characteristics and deter the formation of aluminum carbide (Al_4C_3), a deleterious brittle compound [17].

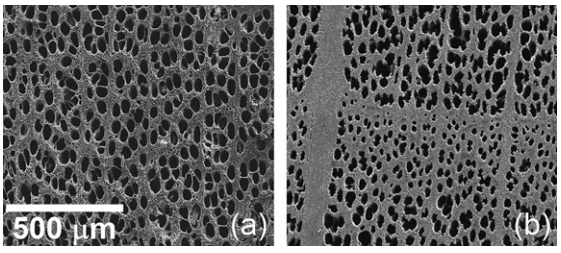

Figure 2. Transverse section of (a) pyrolyzed beech and (b) beech bioSiC [3].

For pressurized infiltration, the specimens were placed into a graphite sample holder within a graphite crucible. A cast Al–13Si–9Mg cylinder was placed in the crucible on top of the bioSiC specimen. A gas-pressure, liquid–metal infiltration apparatus [18,19] was used to heat the specimen to 750 °C in vacuum. A lower temperature was used for the pressurized infiltration because there was less dependence on spontaneous wetting due to the applied argon pressure, and the temperature needs to be only high enough to ensure complete melting of the Al–13Si–9Mg. After a 45 min hold, the furnace was pressurized to 3.5 MPa with ultrahigh-purity argon that forced the molten metal into the porous bioSiC. In order to study the anisotropy of the composites, specimens were machined with the 8 mm dimension both parallel and perpendicular to the axial direction. Images of transverse and longitudinal sections are shown in Figure 4. A universal testing machine (Sintech 20/G, MTS Systems Corp., Eden Prairie, MN) was used to load the specimens along the 8 mm dimension at a rate of 100 μm/min. Compression strength of the specimens was calculated as the maximum recorded load divided by specimen cross-sectional area. Two separately infiltrated $25 \times 25 \times 10$ mm^3 bioSiC pieces were used for mechanical testing, one for axially loaded specimens and one for radially loaded specimens. Specimens from a third pressurized infiltration experiment were used for stiffness measurements using the ultrasonic pulse echo technique.

Longitudinal and shear wave 5 MHz transducers and an ultrasonic inspection system (Matec Instrument Companies, Northborough, MA) were used to measure the sound velocity by the time of flight (TOF) method through samples measuring $4 \times 4 \times 8$ mm^3. Orthorhombic symmetry was assumed and nine measurements were made: one longitudinal and two shear measurements for each principal direction. Error in the diagonal elastic stiffnesses was calculated as the standard deviation of 10 separate TOF measurements. The sample–couplant–transducer bond was completely broken between measurements. Two coupling materials were used: glycerin for longitudinal wave measurements and molasses for shear wave measurements.

The TOF measurements were used to calculate the elastic stiffness matrix, C_{ij}. Longitudinal wave measurements were used to calculate C_{11}, C_{22} and C_{33}, according to

$$C_{ii} = \rho v_{ii}^2, \tag{2}$$

where ρ is the specimen density and the velocity, v, is twice the specimen thickness divided by the sound TOF [20]. The first and second velocity subscripts denote the propagation and polarization directions, respectively, according to Figure 1. Shear wave measurements were used to calculate C_{44}, C_{55}, and C_{66}, where:

$$C_{44} = \rho v_{23}^2, \quad C_{55} = \rho v_{13}^2, \quad C_{66} = \rho v_{12}^2. \tag{3}$$

In order to calculate the elastic compliance matrix, S_{ij}, the three off-diagonal elastic stiffnesses were estimated by assuming transverse isotropy and using the relationship:

$$C_{12} = C_{11} - 2C_{66}. \tag{4}$$

An accurate calculation of the off-diagonal constants, C_{12}, C_{13} and C_{23}, would require specimens oriented in nonprinciple directions [21]. Standard propagation of error was used to calculate the error in C_{12}, C_{13} and C_{23}, which were assumed to be equal. The C_{ij} matrix was inverted to obtain the elastic compliance matrix, S_{ij}, which was used to calculate values for the Young's moduli E_{11}, E_{22} and E_{33} [21] which correspond to E_{Radial}, $E_{\text{Tangential}}$ and E_{Axial}, respectively.

Figure 2(b) shows that the porous bioSiC retains the general structure of the original beech-derived carbon preform. The C → SiC reaction (Eq. (1)) results in a volume change of 43% that closes the smaller fiber and ray channels in the processing of beech wood. There is no significant dimensional change in specimens because the volume expansion is accommodated by the open channels.

While pressureless infiltration of bioSiC in vacuum resulted in little infiltration of the 3 mm thick samples, pressureless infiltration in a nitrogen atmosphere produced partial infiltration. For the specimen shown in Figure 3, infiltration through the 3 mm thickness was achieved after a 1 h hold at 900 °C. These results showed that the PRIMEX™ process is a possible method to make bioSiC-reinforced Al MMCs, but that making larger samples would most likely require longer processing times.

The composite resulting from pressure-infiltration of bioSiC with Al–13Si–9Mg is shown in Figure 4. As expected, Al_4C_3 was not found in any micrographs due to the large amount of silicon in the alloy. The Al–13Si–9Mg melt infiltrated most of the channel space, but some porosity remained in the composites. Possible causes of the residual porosity include an insufficient gas pressure and closed bioSiC preform porosity resulting from the volume expansion during the reaction in Eq. (1). A majority of the remaining porosity occurs in regions of the bioSiC preform that were not converted from carbon to SiC. The amount of residual carbon found in beech-derived bioSiC used in this study averaged 12 vol.% [3]. Residual carbon may occur if there is insufficient silicon reactant or if the processing time is not long enough to allow complete reaction according to Eq. (1). It has been shown that aluminum, Al–Si and Al–Mg alloys do not wet carbon in vacuum at the temperature used [22]. While the pressurization to 3.5 MPa results in near complete infiltration of the bioSiC, the pressure could be too low to force wetting of the unreacted carbon regions. The residual carbon and residual porosity are expected to reduce the composite strength and modulus.

Stress–strain curves showed deviations corresponding to about 0.1% plastic strain before reaching ultimate load. The corresponding strength of both axially and radially loaded samples are summarized in Table 1. The bioSiC preform strength is highly anisotropic, being larger by a factor of 16 in the axial direction as compared to the radial direction. The presence of the aluminum alloy in the channels results in higher axial compressive strength and a significantly higher radial strength (by a factor 16), but at the expense of a 70% higher average density. Large standard deviations in strength values are most likely due to the heterogeneous nature of the wood starting material that is manifest in the composites.

Table 2 provides measured elastic constants for bioSiC/Al–13Si–9Mg MMCs (with equal volume fractions of metal and ceramic and 6.3% residual porosity), as well as the resulting axial and transverse Young's moduli. In addition to Eq. (4), conditions for transversely isotropic materials are $C_{11} = C_{22}$ and $C_{44} = C_{55}$. Although

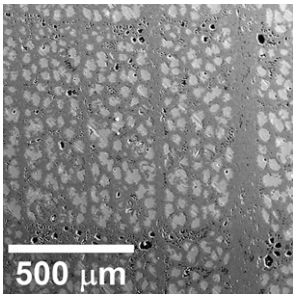

Figure 3. Transverse section of pressureless melt-infiltrated beech bioSiC (light-phase is metal).

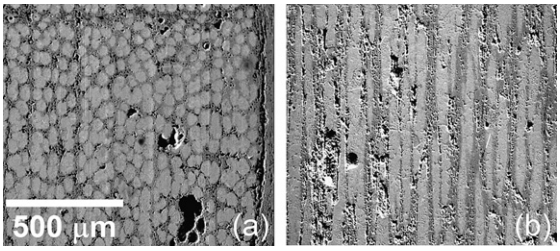

Figure 4. (a) Transverse and (b) longitudinal sections of pressure-infiltrated beech bioSiC (light-phase is metal).

Table 1. Microstructural characteristics and strength of bioSiC and bioSiC–Al composites

Material	Loading direction	Apparent specific gravity[a] (g/cm^3)	Open porosity[a] (%)	SiC fraction (vol.%)	Compressive strength (MPa)
Porous bioSiC [3]	Axial	3.04 ± 0.05	53.2 ± 1.3	100	401 ± 95
Al–13Si–9Mg/bioSiC	Axial	2.72 ± 0.03	11.6 ± 3.5	53	563 ± 79
Porous bioSiC [3]	Radial	3.04 ± 0.05	53.2 ± 1.3	100	25 ± 3
Al–13Si–9Mg/bioSiC	Radial	2.76 ± 0.05	3.0 ± 1.5	48	405 ± 53

[a] Determined by Archimedes' method (ASTM C373-88) on machined 4 × 4 × 8 mm^3 specimens.

Table 2. Elastic properties of composites (equal fractions of bioSiC and Al–13Si–9Mg, and 6.3% porosity) resulting from pulse echo measurements

	C_{ij} (GPa)	E_{ii} (GPa)	ROM (GPa)
11	155 ± 3	119	126
22	124 ± 3	91	126
33	197 ± 3	158	204
44	56 ± 4		
55	55 ± 2		
66	47 ± 4		
12	62 ± 5		
13	62 ± 5		
23	62 ± 5		

C_{11} and C_{22} differ by more than 30 GPa, transverse isotropy was assumed for the sake of simplicity. These results can be compared to the rule of mixtures (ROM) calculations:

$$E_{\text{Axial}} = E_{\text{SiC}} V_{\text{SiC}} + E_{\text{Al}} V_{\text{Al}} \tag{5}$$

$$E_{\text{Transverse}} = \left[\frac{V_{\text{SiC}}}{E_{\text{SiC}}} + \frac{V_{\text{Al}}}{E_{\text{Al}}} \right]^{-1}, \tag{6}$$

where E is the Young's modulus and V is the volume fraction. Using 330 GPa for E_{SiC} [23], 78 GPa for E_{Al} (measured by pulse echo) and 0.50 for V_{SiC} and V_{Al}, E_{Axial} and $E_{\text{Transverse}}$ have values of 204 and 126 GPa, respectively. These values are estimates because the ROM calculations apply to uniaxial fiber composites (unlike the present reticulated bioSiC architecture) and they take neither residual porosity nor unreacted carbon into account. Modulus values for the porous bioSiC (47 vol.% SiC), $E_{\text{Axial}} = 116$ GPa and $E_{\text{Radial}} = 16$ GPa [3], indicate the same trend observed in compression strength: the effect of filling the channels with aluminum leads to large improvements in the transverse direction and a concomitant reduction in anisotropy.

The experimental results also show a difference in the transverse moduli: $E_{\text{Radial}} = 119$ GPa and $E_{\text{Tangential}} = 91$ GPa. A possible explanation for this difference can be drawn from the properties of the wood starting material. Wood is typically stiffer when loaded radially as opposed to tangentially [8]. The rays, visible as vertical bands in Figures 2(b) and 3, have a higher density than the surrounding channels and act as reinforcements when loading is in the radial direction. The same reasoning can be used for the composite materials because the structure of the wood is maintained throughout the process steps leading to the composites.

The measured longitudinal modulus corresponds well to published results of SiC particle-reinforced aluminum MMCs prepared by pressureless infiltration [24]: for SiC fractions of 41–54 vol.% and residual porosity of 3–8 vol.%, Young's moduli for the composites are reported in the range of 165–226 GPa. In contrast to the production of SiC particles, relatively low-temperatures are used to fabricate bioSiC and the microstructure and pore size distribution of the SiC preform are known based on the precursor wood. However, the resulting bioSiC composites exhibit low-transverse modulus and only small amounts of plastic strain.

In summary, melt infiltration, whether pressureless or pressurized, is an effective method of producing bioSiC-reinforced aluminum MMCs. The compressive strength and stiffness of the composites was found to be greater than that of the porous bioSiC preforms, especially in the transverse direction. This leads to a reduction in the anisotropy in strength and stiffness of the composites, as compared to the porous bioSiC, but at the expense of increased density and very limited high-temperature use.

This work is supported by the National Science Foundation Grant DMR-0244258. T.E.W. was supported by a National Defense Science and Engineering Graduate Fellowship.

[1] P. Greil, T. Lifka, A. Kaindl, J. Eur. Ceram. Soc. 18 (1998) 1961.
[2] A. Herzog, U. Vogt, O. Kaczmarek, R. Klinger, K. Richter, H. Thoemen, J. Am. Ceram. Soc. 89 (2006) 1499.
[3] V.S. Kaul, K.T. Faber, R. Sepulveda, A.R. de Arellano-Lopez, J. Martinez-Fernandez, Mater. Sci. Eng. A. 428 (2006) 225.
[4] J. Cao, C.R. Rambo, H. Sieber, J. Porous Mater. 11 (2004) 163.
[5] J. Cao, O. Rusina, H. Sieber, Ceram. Int. 30 (2004) 1971.
[6] C.R. Rambo, J. Cao, O. Rusina, H. Sieber, Carbon 43 (2005) 1174.
[7] C.R. Rambo, J. Cao, H. Sieber, Mater. Chem. Phys. 87 (2004) 345.
[8] L.J. Gibson, M.F. Ashby, Cellular Solids: Structure and Properties, second ed., Cambridge University Press, Cambridge, 1997.
[9] E. Wheeler, in: K.H. Jürgen Buschow, R.W. Cahn, M.C. Flemings, B. Ilschner, E.J. Kramer, S. Mahajan (Eds.), Encyclopedia of Materials: Science and Technology, Elsevier, New York, 2001, p. 9653.
[10] A.R. de Arellano-Lopez, J. Martinez-Fernandez, P. Gonzalez, C. Dominguez, V. Fernandez-Quero, M. Singh, Int. J. Appl. Ceram. Technol. 1 (2004) 56.
[11] M. Presas, J.Y. Pastor, J. Llorca, A.R. de Arellano-Lopez, J. Martinez-Fernandez, R.E. Sepulveda, Scripta Mater. 53 (2005) 1175.
[12] C. Zollfrank, N. Travitzky, H. Sieber, T. Selchert, P. Greil, Adv. Eng. Mater. 7 (2005) 743.
[13] A. Mortensen, V.J. Michaud, M.C. Flemings, JOM-J. Miner. Met. Mater. Soc. 45 (1993) 36.
[14] G.H. Schiroky, D.V. Miller, M.K. Aghajanian, A.S. Fareed, Key Eng. Mater. (1997) 141.
[15] D.R. White, A.W. Urquhart, M.W. Aghajanian, D.K. Creber, US Patent 4,828,008, 1989.
[16] M.K. Aghajanian, M.A. Rocazella, J.T. Burke, S.D. Keck, J. Mater. Sci. 26 (1991) 447.
[17] M.I. Pech-Canul, R.N. Katz, M.M. Makhlouf, Metall. Mater. Trans. A 31 (2000) 565.
[18] J.T. Blucher, J. Mater. Process. Technol. 30 (1992) 381.
[19] C.S. Marchi, M. Kouzeli, R. Rao, J.A. Lewis, D.C. Dunand, Scripta Mater. 49 (2003) 861.
[20] M.J.P. Musgrave, Crystal Acoustics: Introduction to the Study of Elastic Waves and Vibrations in Crystals, Holden-Day, San Francisco, 1970.
[21] H.M. Ledbetter, D.T. Read, J. Appl. Phys. 48 (1977) 1874.
[22] C.R. Manning, T.B. Gurganus, J. Am. Ceram. Soc. 52 (1969) 115.
[23] V. Kaul, Unpublished research.
[24] M.I. Pech-Canul, M.M. Makhlouf, J. Mater. Synth. Process. 8 (2000) 35.